Materials Advances

Accepted Manuscript

This article can be cited before page numbers have been issued, to do this please use: S. Some, A. Mohan, R. Laha, S. Dhibar, P. Kaith, A. Trivedi, S. Bhattacharjee, T. O. Ajiboye, L. N. Nthunya, A. Bera, A. K. Das, S. K. Panja, S. Dam, P. Predeep and B. Saha, *Mater. Adv.*, 2026, DOI: 10.1039/D6MA00248J.

View Article Online
DOI: 10.1039/D6MA00248J

Development of a Supramolecular Cobalt (II) Metallohydrogel from L-Serine-Based Low Molecular Weight Gelator for Dual Antimicrobial and Semiconducting Applications†

Sangita Some,[a] Aiswarya Mohan,[b] Rajlakshmi Laha,[c] Subhendu Dhibar,[a]* Priya Kaith,[d] Aditi Trivedi,[e] Subham Bhattacharjee,[f] Timothy O. Ajiboye,[g] Lebea N. Nthunya,[h] Ashok Bera,[d] Asit Kumar Das,[i] Sumit Kumar Panja,[j] Somasri Dam,[c]* Padmanabhan Predeep,[k]* Bidyut Saha,[a]*

[a] *Colloid Chemistry Laboratory, Department of Chemistry, The University of Burdwan, Golapbag, Burdwan-713104, West Bengal, India *E-mail: sdhibar@scholar.buruniv.ac.in, Tel: +91 7001575909 (S. Dhibar); *E-mail: bsaha@chem.buruniv.ac.in, Tel: +91 9476341691 (B. Saha).*
[b] *Laboratory for Molecular Photonics and Electronics (LAMP), Department of Physics, National Institute of Technology Calicut, Calicut-673603, Kerala, India.*
[c] *Department of Microbiology, The University of Burdwan, Burdwan-713104, West Bengal, India, *E-mail: sdam@microbio.buruniv.ac.in (S. Dam).*
[d] *Department of Physics, Indian Institute of Technology Jammu, J&K-181221, India.*
[e] *National Institute of Science Education and Research (NISER), Bhubaneswar, Odisha 752050, India.*
[f] *Department of Chemistry, Kazi Nazrul University, Asansol-713303, West Bengal, India.*
[g] *Faculty of Natural and Agricultural Sciences, North-West University, Mmabatho-2735, South Africa.*
[h] *Institute for Nanotechnology and Water Sustainability, University of South Africa, Florida Science Campus, 1709 Roodepoort, South Africa.*
[i] *Department of Chemistry, Murshidabad University, Berhampore-742101, West Bengal, India.*
[j] *Tarsadia Institute of Chemical Science, Uka Tarsadia University, Surat-394350, Gujrat, India.*
[k] *School of Nanoscience and Nanotechnology, Mahathma Gandhi University, Kottayam-686560, Kerala, India; E-mail: predeep@mgu.ac.in (P. Predeep).*

Abstract

A Co(II)-metallohydrogel was synthesized by combining cobalt(II) nitrate and L-serine in the presence of potassium hydroxide in an aqueous medium at room temperature. The resulting hydrogel demonstrated excellent mechanical strength, as confirmed through rheological studies. Field emission scanning electron microscopy (FESEM) and energy-dispersive X-ray (EDX) mapping revealed a hierarchical microstructure and confirmed the presence of essential elements such as Co, C, N, O, and K. FT-IR spectroscopy shed light on the supramolecular interactions involved in gel formation, while powder X-ray diffraction (PXRD) provided information on the material's crystalline features. Optical absorption analysis confirmed the semiconducting nature of the gel, showing notably high electron mobility compared to similar materials. Furthermore, the metallohydrogel exhibited strong antibacterial activity against both Gram-positive (*B. subtilis, S. aureus*) and Gram-negative (*E. coli, P. aeruginosa*) pathogens. These multifunctional properties underscore the material's potential for future applications in both flexible electronics and biomedical technology.

1. Introduction

Gels represent a unique subset of soft materials, notable for their capacity to incorporate large volumes of liquid within a three dimensional network structure.[1] This retention of fluid is enabled by gelator molecules that assemble into a robust framework via various cross linking mechanisms.[2,3] The combination of solid like mechanical strength with the dynamic mobility of a liquid endows gels with remarkable physical and chemical properties. These characteristics make them suitable for diverse applications across biomedical engineering, pharmaceuticals, food processing, cosmetic formulations, and advanced materials development.[4]

View Article Online
DOI: 10.1039/D6MA00248J

Gels are generally classified into two major types based on how their networks are formed: covalently bonded chemical gels and physically assembled supramolecular gels. Chemical gels rely on permanent covalent linkages that produce rigid, often irreversible structures.[5] Conversely, supramolecular gels are formed by the self-assembly of small gelator molecules[6,7]-typically under 3000 Daltons-held together by noncovalent interactions[8-13]

The molecular design of the gelator plays a pivotal role in the gelation process.[14-16]. An extensive variety of LMWGs have been employed to create supramolecular gels, including dicarboxylic acids,[14] urea derivatives,[15] modified amino acids,[16] fatty acids,[5] sorbitol,[17] dendrimers,[17] carbohydrates,[17] and many more. Equally crucial to the gelation process is the role of the solvent, which not only acts as the medium but also directly affects molecular assembly.[17-18] The choice of solvent can significantly impact gel morphology, fiber dimensions, and overall gel stability. Parameters such as polarity, viscosity, hydrogen-bonding capability, and coordination tendencies of the solvent influence the strength and nature of the interactions among the gelator molecules.[14-17] Solvents commonly used ingelation studies include water,[18-23] alcohols,[24] dimethylformamide (DMF),[25] dimethyl sulfoxide (DMSO),[26] acetonitrile,[27] acetone,[28] are among the most effective solvents for initiating supramolecular gel formation.

Metallohydrogels represent a novel and rapidly evolving category within the field of supramolecular gels. These systems are characterized by the integration of metal ions or metal-based complexes that coordinate with organic ligands, facilitating the formation of self-organized three-dimensional networks.[29] Typically, such gels arise from the coordination interactions between low molecular weight gelators (LMWGs) and various transition metal ions, giving rise to hybrid materials with superior functionalities. Transition metals including copper(II),[30] nickel(II),[31,32] cobalt(II),[33] have frequently been employed to construct metallogels. The presence of metal centers not only reinforces the structural integrity of the gel matrix but also introduces diverse functional characteristics such as redox behavior,[34] catalytic activity,[18,19] magnetic properties,[35] and the ability to serve as templates for nanoparticle formation.[36]

Selecting an appropriate ligand is crucial in metallohydrogel synthesis. Ligands possessing multiple functional groups, such as amino, hydroxyl, or carboxylate moieties, are especially effective, with amino acids being prime examples due to their versatile coordination capabilities.[37] Among them, L serine stands out as a promising candidate for constructing metallohydrogels. This naturally derived amino acid features a side chain that includes both amine and hydroxyl groups, enabling strong interactions with metal ions and promoting the assembly of stable supramolecular frameworks. Additionally, its natural abundance and biocompatibility make L serine highly suitable for applications in both biomedical and environmental fields.

Metallogels exhibit antibacterial properties through several distinct mechanisms. One primary mode of action involves the disruption of bacterial cell membranes, which leads to the leakage of vital intracellular contents.

View Article Online
DOI: 10.1039/D6MA00248J

Metallohydrogel-based Schottky diodes are promising for advanced electronics due to their tunable electronic properties, stability, and compatibility with various fabrication techniques. By adjusting metal-ligand combinations, device performance can be optimized. Their integration with other components and environmental durability make them ideal for multifunctional electronic and optoelectronic device applications. In a significant advancement, Dhibar and collaborators developed an efficient and straightforward approach for synthesizing metallogels, eliminating the need for harsh conditions while retaining material functionality.[18,32] Inspired by their strategy, We report the synthesis of a novel L-serine–derived metallohydrogel, in which L-serine acts as a tridentate (N, O, O) ligand.[38] The gel formation occurs through coordination of Co(II) ions with the amino nitrogen, caboxylate oxygen, and hydroxyl oxygen groups of the ligand under alkaline conditions (pH ≥ 10).[39] This gel forms swiftly in an aqueous environment, yielding a stable blue coloured material. The gel network is predominantly stabilized through coordination interactions between Co (II) ions and serine, complemented by intermolecular hydrogen bonding among gelator units. The resulting hydrogel demonstrates remarkable stability, uniform structure, and reproducibility, positioning it as a strong candidate for future functional materials. However, systematic studies on cobalt-L serine based metallohydrogels remain limited, particularly regarding coordination driven gelation mechanisms and their influence on multifunctional properties.[40]

This Co (II) based metallohydrogel displays excellent electrical conductivity and notable-optoelectronic behaviour, along with pronounced antibacterial efficacy against various pathogenic strains. Comprehensive analyses of its rheological performance and internal morphology have been carried out. Designed around a metal semiconductor junction, the material shows efficient charge transport properties, highlighting its applicability in semiconducting devices.

2. Experimental

2.1. Materials. Cobalt (II) nitrate hexahydrate (Sigma-Aldrich, USA, 99.99% trace metals basis), L-serine (Sigma-Aldrich, USA, 99%), and Potassium hydroxide (Merck, 98%) were utilized as received. Dry DMF solvent was employed throughout the study. Tryptone, D-(+)-Glucose anhydrous, and Yeast Extract Powder were obtained from Himedia..

2.2. Apparatus and measurements.

2.2.1 Rheological analysis. Rheological measurements were conducted with the gap between the cone and plate set at 0.5 mm. The gel samples were carefully placed on the rheometer plate. A strain amplitude sweep was carried out at a fixed oscillation frequency of 1 Hz, covering a strain range from 0.001% to 100% at 25 °C. To evaluate the material's viscoelastic behavior, frequency sweep experiments were subsequently performed within the linear viscoelastic region (LVR) at a constant strain of 0.01%, ensuring that the measured parameters reflect the undisturbed network structure of the gels.

View Article Online
DOI: 10.1039/D6MA00248J

2.2.2 FESEM study. The metallohydrogel was gently drop-cast onto a thoroughly cleaned glass substrate and left to air dry overnight. After drying, the samples were coated with a thin layer of gold via vapor deposition. Scanning electron microscopy (SEM) was performed using a Carl Zeiss SUPRA 55VP at an accelerating voltage of 10-15 kV, while elemental analysis was carried out using EDX on a ZEISS EVO 18 system.

2.2.3 FT-IR study. IR spectra in the 4000-500 cm^{-1} range of the samples pelleted in KBr were recorded either on a JASCO FTIR 4700 spectrophotometer.

2.2.4 PXRD study. A PANalytical X'Pert powder X-ray diffractometer using Cu Kα1 radiation was utilized to analyze the nature of the metallohydrogel.

2.2.5 IV characteristics. The IV characteristics of the device were recorded using a Keithley 2400 source meter connected to a computer.

2.3. Synthesis of Co (II)-L-serine based metallohydrogel (Co-LS).

An aqueous solution of bright pink cobalt (II) nitrate hexahydrate (0.291 g, 1 mmol, ~1 mL) was swiftly combined with a clear aqueous solution (~1 mL) containing L-serine (0.105 g, 1 mmol) and 0.5 equivalents of potassium hydroxide at ambient temperature. This immediate mixing led to the rapid formation of a deep blue cobalt (II)-based metallohydrogel, referred to as Co-LS. A schematic illustration of the proposed Co-LS network and an inverted vial image showcasing its gel state stability are shown in Figure 1. The successful gelation and mechanical integrity of the Co-LS metallohydrogel were initially confirmed via the inverted vial method (Figure 1) and further substantiated by rheological investigations (detailed below). To determine the minimum gelation threshold, the minimum gelation concentration (MGC) of the Co-LS system was evaluated by systematically varying the concentrations of $Co(NO_3)_2 \cdot 6H_2O$ and L-serine from 20 to 150 mg/mL, keeping their mass ratio constant at 1:1. At 150 mg/mL concentration of each component in water, a uniform and stable deep blue gel was consistently formed. Thermal stability of the gel was assessed using a digital melting point apparatus. The Co-LS metallohydrogel retained its structure until a transition into the sol phase occurred at approximately 80 ± 2 °C, indicating a high thermal resistance. Additionally, the pH of the Co-LS gel was measured using a Mettler Toledo FP20 pH meter, revealing that the gel system forms and remains stable at pH values of 10 or higher.

View Article Online
DOI: 10.1039/D6MA00248J

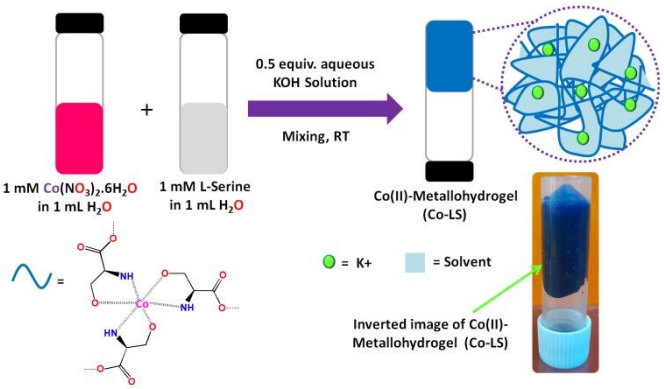

Fig. 1. The gelation process proceeds according to the described synthetic route, culminating in the formation of the Co(II)-based metallohydrogel (Co-LS). A photographic image alongside a schematic illustration is provided to visually represent the resulting Co-LS metallohydrogel.

2.4. Antimicrobial activity of Co-LS.

Quantitative assessment of antimicrobial effect of Co-Ls was carried out with a series of concentrations of the metallogel on different bacterial strains such as *Escherichia coli, Bacillus subtilis, Pseudomonas aeruginosa,* and *Staphylococcus aureus*. Among them, *Pseudomonas aeruginosa* and *Escherichia coli* are Gram-negative in nature, whereas *Staphylococcus aureus* and *Bacillus subtilis* are Gram-positive. The concentrations of Co-Ls used for the experiment were 20mg/ml, 40mg/ml, 60mg/ml, 80mg/ml, and 100mg/ml. 100µl of inoculum from log phase culture of each bacterial strain was spread uniformly on TGA (1% tryptone, 1% glucose, 1% yeast extract and pH 6.5) agar plate with the help of sterile cotton swabs. Later, 10µl of metallogel suspension from each concentration was spotted on the agar surface with bacterial inoculum spread on it. Broad-spectrum antibiotic Streptomycin was used as positive control for this experiment. The positive control was spotted too on each plate. The plates were incubated at 37°C for 24 hours. All the experiments are performed in triplicate.

3. Results and discussion

3.1. Rheological Analysis

To evaluate the mechanical strength and viscoelastic behaviour of the Co-LS metallohydrogel, rheological measurements were carried out using a rheometer. Both angular frequency sweep and strain-sweep tests were conducted on the sample prepared at the minimum gelation concentration (MGC) of 424 mg/mL for $Co(NO_3)_2 \cdot 6H_2O$ and L-serine. The gel-like nature of the material was confirmed by the dominance of the storage modulus (G') over the loss modulus (G''), indicating its semi-solid, elastic characteristics. Specifically, the storage modulus (G') exhibited significantly higher values than the loss modulus (G'') across the frequency range tested, a typical signature of viscoelastic gels (Figure 2a). The

View Article Online
DOI: 10.1039/D6MA00248J

average G' was observed to be greater than 10^2 Pa, suggesting a mechanically robust network stabilized by Co(II)-serine coordination and non-covalent interactions. Furthermore, strain-sweep experiments were performed at a constant angular frequency of 6.283 rad/sec to assess the structural integrity of the hydrogel under increasing strain. As shown in Figure 2b, the gel maintained its mechanical integrity over a broad range of strain values before yielding, reflecting its high strain tolerance. These findings demonstrate that the Co-LS metallohydrogel possesses excellent mechanical stability, making it a strong candidate for practical applications in soft materials and flexible electronic devices.

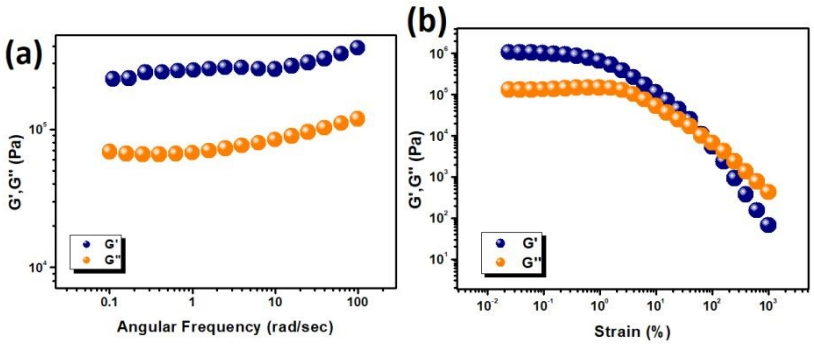

Fig. 2. (a) Angular frequency measurements vs G' and G'' of Co-LS metallohydrogel; (b) Strain-sweep measurements of Co-LS metallohydrogel performed at a constant frequency of 6.283 rad/sec.

3.2. Study of Morphology

Field emission scanning electron microscopy (FESEM) analysis of the Co-LS metallohydrogel reveals a well-defined hierarchical flake-like network structure (Figure 3a). This intricate morphology results from the coordination of $Co(NO_3)_2 \cdot 6H_2O$ with L-serine in an aqueous medium. The observed microstructure is attributed to strong supramolecular interactions, which play a vital role in stabilizing the gel framework. The fibrous morphology of the gel facilitates the charge transfer mechanisms. The porous network enhances the surface area availability which helps for interaction with microbial cells. These properties contribute to the observed semiconducting behaviour and antibacterial activity of the metallogel.f Elemental mapping performed on a selected region confirms the uniform distribution of key components, including cobalt, L-serine, and potassium hydroxide. EDX further supports these findings, detecting the presence of carbon (C), nitrogen (N), oxygen (O), potassium (K), and cobalt (Co) elements within the metallohydrogel matrix (Figure 3b-g). These results collectively validate the successful incorporation of the gel's primary constituents into a stable, interconnected supramolecular network, highlighting the material's compositional integrity and structural uniformity.

View Article Online
DOI: 10.1039/D6MA00248J

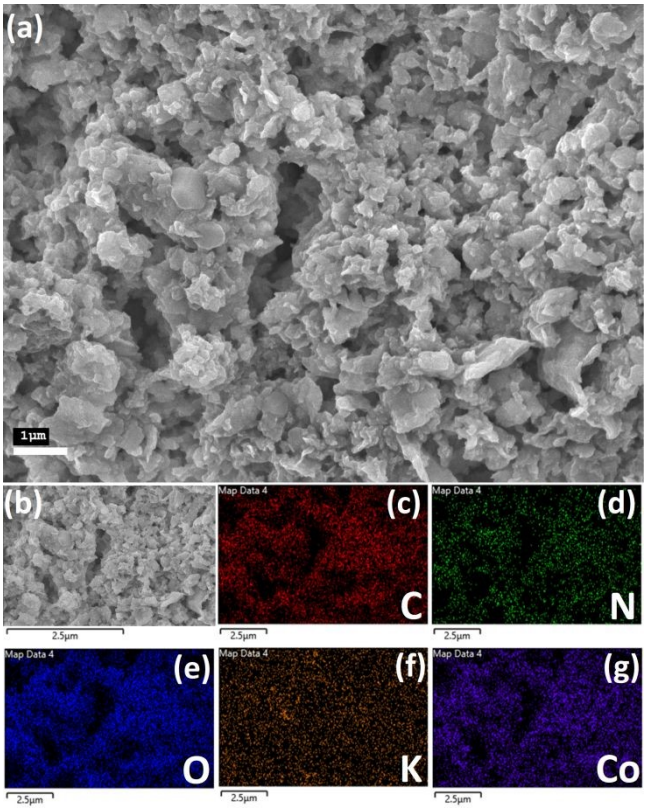

Fig. 3. (a) FESEM analysis reveals the microstructural features of the Co-LS metallohydrogel, (b-g) the elemental mapping of Co-LS metallohydrogel showing the presence of C, N, O, K and Co elements.

3.3. FT-IR analysis of Co-LS Metallohydrogel

Fourier Transform Infrared spectroscopy is an essential tool for investigating the functional groups and molecular interactions in metallogels. Figure 4 shows the comparative FTIR spectra of Cobalt nitrate hexahydrate, L-serine and Cobalt-L Serine metallohydrogel. The spectrum of cobalt nitrate appears at ~3400 cm^{-1} assigned to coordinated water molecules along with band around 1370 cm^{-1} attributed to stretching mode of nitrate ion. The spectrum of L -Serine exhibits a broad band around 3200-3400 cm^{-1} assigned to the overlapping of $-NH_2$ and -OH stretching vibrations while asymmetric and symmetric stretching mode of carboxylate (COO-) group appear at 1600 and 1400 cm^{-1} respectively. After metallogel formation the asymmetric stretching band of carboxylate group shifts to 1570 cm^{-1} and symmetric band 1370 cm^{-1}. The change in ($\Delta\nu_{COO^-}$) i.e., (ν_{as}–ν_s), indicate the coordination of carboxylate oxygen atom of L serine with Co^{2+} ion. On the other hand, the broad -NH/-OH become less intense and broader that implies the involvement of these groups in H bonding and metal ion coordination. The characteristic nitrate peak observed in $Co(NO_3)_2.6H_2O$ becomes significantly weaker, confirming an alternation in its coordination environment. These findings collectively confirm the successful formation of cobalt-L serine (Co-LS) metallogel network.

View Article Online
DOI: 10.1039/D6MA00248J

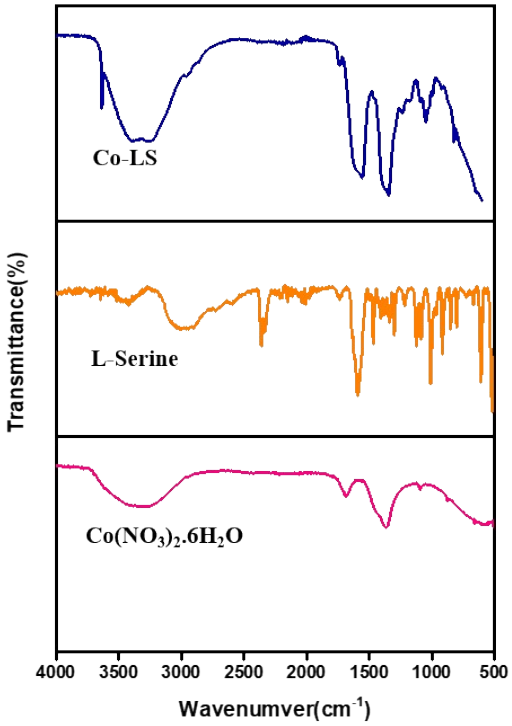

Fig. 4. FT-IR spectra of the xerogel form of Co-LS metallohydrogel, L-serine gelator and Cobalt nitrate

3.4. PXRD analysis of Co-LS Metallohydrogel

PXRD analysis of the Co-LS metallohydrogel was performed to examine its structural organization and crystalline features. The diffraction pattern, recorded over the 2θ range of 5°–80°, exhibits distinct reflections at 19.2°, 23.7°, 29.6°, 32.6°, 38.7°, 41.2°, 41.9°, and 48.3°, indicating the presence of ordered domains within the metallohydrogel network.

PXRD measurements were conducted on the as-prepared gel without post-synthetic removal of KOH to preserve structural integrity. The diffraction features observed at 2θ values of 27.4°, 29.6°, 33.8°, 34.6°, and 38.7°, which are consistent with reported reflections of KOH, are attributed to residual alkaline species associated with the gel matrix.

Minor shifts in peak positions compared to pristine starting materials can be attributed to coordination-driven reorganization, hydrogen bonding interactions, and changes in lattice parameters occurring during gelation.

View Article Online
DOI: 10.1039/D6MA00248J

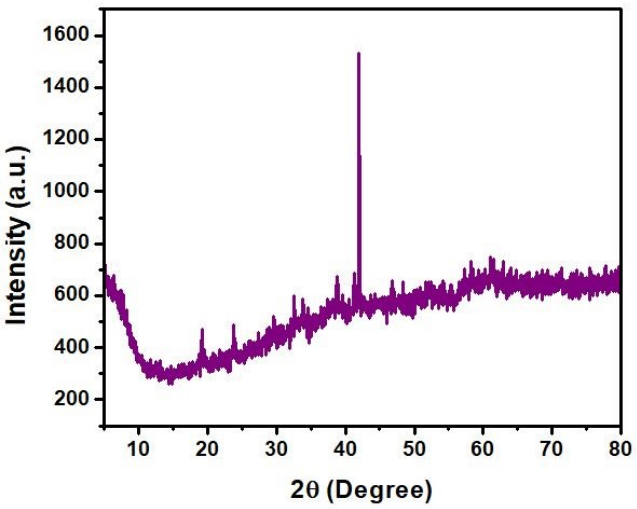

Fig. 5. PXRD pattern of the Co-LS metallohydrogel.

3.5. Thin film deposition and Device assembly

For assessing the electrical transport behavior and exploring the feasibility of the Co-LS metallohydrogel in semiconductor applications, forming a continuous thin film on conductive substrates such as Indium Tin Oxide (ITO) is crucial. However, due to the intrinsic viscoelastic nature of the gel, achieving a uniform coating is challenging. To mitigate this issue, Polymethylmethacrylate (PMMA) serves as a structural support, enabling effective dispersion of the gel in N,N-Dimethylformamide (DMF) and improving its film-forming properties.

The process begins with dissolving PMMA in DMF at 40°C while stirring for two hours. Different concentrations of PMMA, ranging from 10 to 50 wt.%, are incorporated into the gel and mixed for an additional four hours to examine the feasibility of film formation. The results indicate that a 50 wt. % PMMA mixture produces the most homogeneous films, ensuring complete substrate coverage with minimal surface irregularities. In contrast, increasing the PMMA content beyond this threshold negatively impacts film integrity, leading to structural inconsistencies. Before deposition, ITO glass substrates undergo a rigorous cleaning process. The Co-LS-PMMA blend is then uniformly distributed over the substrate via spin-coating at 1000 rpm for 50 seconds, immediately followed by annealing at 60°C for five minutes. To complete the assembly, a thin aluminum layer (100 nm) is deposited using a vacuum evaporation technique, creating a layered configuration of ITO/Co-LS-PMMA/Al. The electrical behavior of the resulting thin film device is subsequently evaluated through current-voltage (I-V) measurements.

3.6 Optical Characterization

To determine the optical band gap, the optical absorbance spectrum of the synthesized metallogel was recorded. The UV-Vis absorption spectrum in the wavelength range of 200-800 nm is presented in Fig 6 (inset). The direct optical band gap energy of the metallogel was estimated using the following Tauc equation (i)

View Article Online
DOI: 10.1039/D6MA00248J

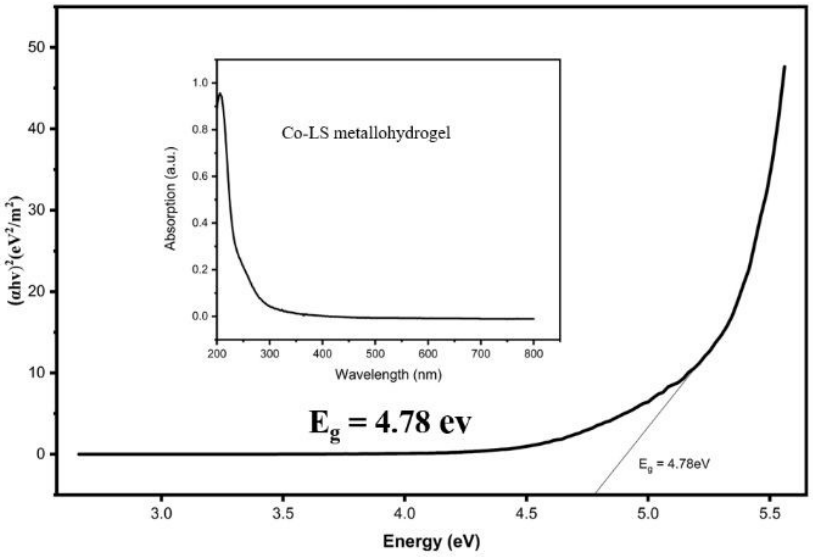

Fig. 6. Tauc's Plot to evaluate the band gap energy and UV-Vis absorption spectra of the metallogel

$$(\alpha h\nu)^2 = c(h\nu - E_g) \quad \text{..... (i)}$$

where α, E_g, h, υ stands for absorption coefficient, the optical band gap energy, Planck's constant and frequency and c refer a constant. From the extrapolation of the linear region of the $(\alpha h\nu)^2$ vs hν plot the calculated band gap (E_g) of the Co-LS metallogel is measured as 4.78 eV.

3.7 Charge Transport Analysis and Thin Film Device Performance.

The electrical characterization of the fabricated device was conducted through current-voltage (I-V) measurements usig a Keithley 2450 source meter. A bias voltage was applied within the range of 0 to ±2V to evaluate the device's response. The resulting I-V characteristics for the device are illustrated in Figure 7.

View Article Online
DOI: 10.1039/D6MA00248J

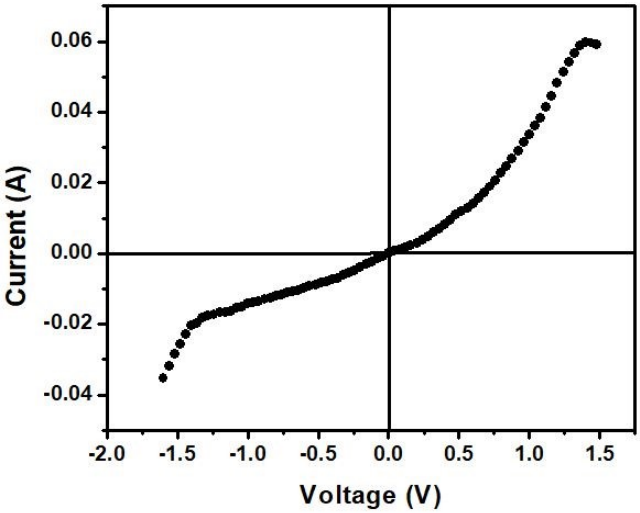

Fig. 7. I-V characteristics of Co-LS metallohydrogel based diode.

The gel-based device demonstrates I-V characteristics comparable to those of a Schottky diode. The essential diode parameters are extracted using Cheung's method,[41] and the I-V behavior is analyzed within the framework of Thermionic Emission theory. The corresponding standard equations are provided below.

$$I = I_0\left(\frac{qV}{\eta KT}\right)\left[1 - \exp\left(\frac{-qV}{\eta KT}\right)\right] \quad (1)$$

$$I_0 = AA^*T^2 \exp\left(\frac{-q\varphi_B}{\eta KT}\right) \quad (2)$$

In this formulation, V is the applied bias voltage, k is the Boltzmann constant and q denotes the charge of an electron. The temperature is expressed in Kelvin as T, while I_0 corresponds to the reverse saturation current. The effective diode area is given by A,and the Richardson constant A^*, is assumed to be $32AK^{-2}cm^{-2}$.

The extraction of the ideality factor (η), barrier height (φ_B), and series resistance (R_s) is conducted using Cheung's method, which relies on the analysis of the forward bias I-V characteristics. The method employs differential techniques to linearize the nonlinear response of the diode, facilitating accurate parameter estimation. The series resistance is determined from the slope of the modified function (dV/dln I) versus current (Figure 8). The barrier height is subsequently calculated using the extracted parameters in conjunction with the thermionic emission model. The governing equations for these calculations are provided below.

$$\frac{dV}{d(lnI)} = \left(\frac{\eta KT}{q}\right) + IR_s \quad (3)$$

$$H(I) = V - \left(\frac{\eta KT}{q}\right)\ln\left(\frac{I}{AA^*T^2}\right) \quad (4)$$

View Article Online
DOI: 10.1039/D0MA00248J

Figure 8 below shows the H(I) vs I plot and as seen from the above equations, the slope and intercept of this plot combined with the ideality factor values can be used to determine the value of barrier height(φ_B). Figure 9 presents the H(I) versus I plot, which serves as a crucial tool for extracting the barrier height(φ_B). As derived from the preceding equations, the slope and intercept of this plot, in conjunction with the ideality factor (n), facilitate the precise determination of (φ_B).

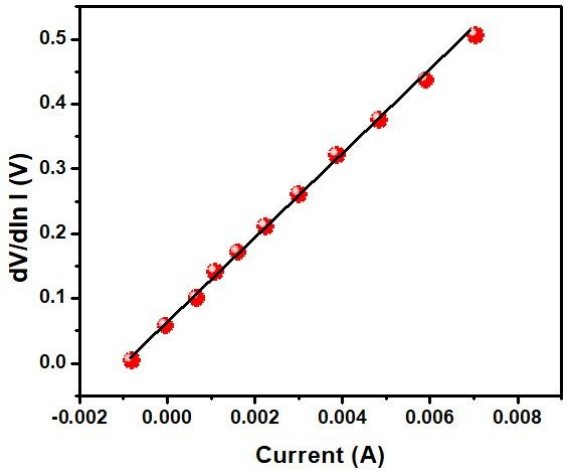

Fig. 8. $\frac{dV}{d(\ln I)}$ vs I plot of Co-LS metallohydrogel based schottky diode.

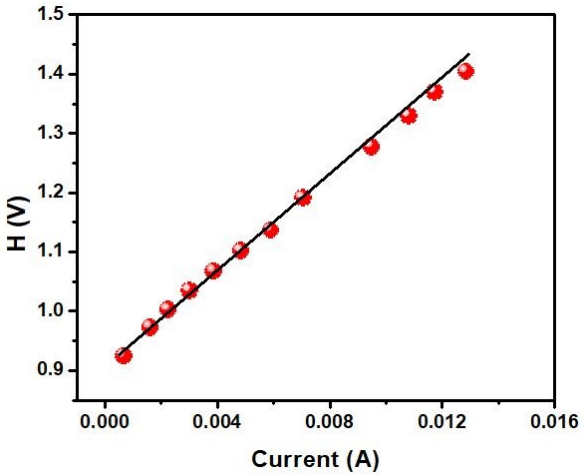

Fig. 9. H vs I plot of Co-LS metallohydrogel based Schottky Diode.

Table 1. The estimated values of ON/OFF ratio, Conductivity, Ideality factor, Barrier potential, and Series resistance of the metallohydrogel.

							Series Resistance (Ω)	Mobility (cm^2/Vs)

View Article Online
DOI: 10.1039/D5MA00248J

Conductivity (Sm^{-1})	Ideality Factor	Barrier Height (eV)	dV/dlnI vs I	H(V) vs I	
9.45	1.83	0.47	58.94	46.62	1.97×10^{-5}

In this study, the charge carrier mobility was determined using the well-established Mott-Gurney equation,[42] which is commonly employed for space-charge-limited current (SCLC) analysis in organic and semiconductor devices.

$$I = \frac{9}{8}\epsilon_r \epsilon_0 \mu A \frac{V^2}{d^3} \qquad (5)$$

In this equation, ϵ_0 represents the permittivity of free space, while ϵ_r denotes the dielectric constant of the material blend. The parameter μ corresponds to the charge carrier mobility, and d is the thickness of the film.

The charge carrier mobility is extracted using the Mott-Gurney equation by analyzing the double logarithmic I-V plots of the devices, as shown in Figure 10. This approach enables the identification of different conduction regimes and the determination of mobility in the space-charge-limited current (SCLC) region.

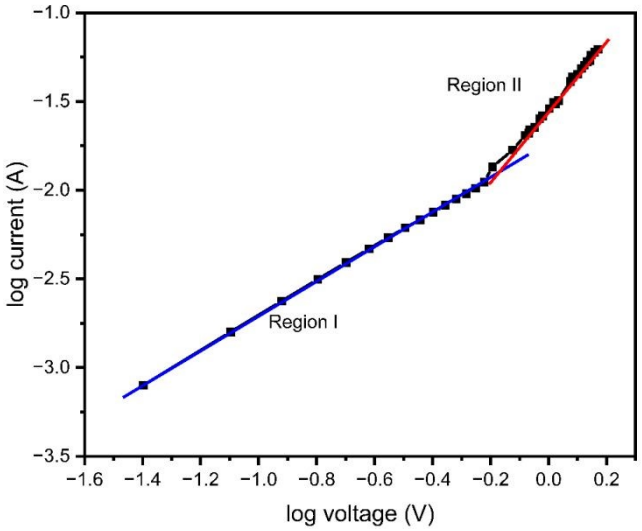

Fig. 10. log I vs log V Co-LS metallohydrogel based Schottky Diode.

In the ohmic region (Region I), the current exhibits a direct proportionality to the applied voltage, as shown in Figure 10. Conversely, in the space-charge-limited current (SCLC) region (Region II), the

View Article Online
DOI: 10.1039/D6MA00248J

current follows a quadratic dependence on voltage.[43,44] Therefore, Region II, identified in the figure, is utilized for mobility calculations. The segments of the curve exhibiting a slope of 2 (Region II) are specifically fitted to the Mott-Gurney equation (Eq. No. 5) to extract the charge carrier mobility values. In comparison to the traditional inorganic or organic semiconductors the mobility is (1.97×10^{-5} cm² V^{-1} s^{-1}) is low. However, the main goal of this work is to demonstrate semiconducting functionality in a soft, supramolecular metallohydrogel system rather than to compete with advanced semiconductors. Such values are typical of soft, supramolecular, and hydrogel-based semiconductors, where charge transport is governed by hopping and percolation through disordered metal–ligand networks and hydrated domains rather than band-like transport. For low-frequency and low-current applications, such as chemical and biosensors, soft rectifiers, and bio integrated electronic interfaces, comparable mobilities have been widely reported for metallogels and hydrogel-based electronic materials. In these systems, mechanical compliance, processability, and multifunctionality are often more critical than high charge carrier mobility.[45,46]

3.8. Inhibiting Activity for pathogens

Co-LS demonstrated strong antimicrobial activity against both Gram-positive (*Bacillus subtilis, Staphylococcus aureus*) and Gram-negative (*Escherichia coli, Pseudomonas aeruginosa*) bacterial strains, as shown in Figure 11. Streptomycin was used as a positive control at a concentration of 0.1 mg mL^{-1}, which falls within the standard range for antibacterial assays. The Co-LS metallohydrogel was tested at 100 mg mL^{-1} to ensure sufficient diffusion and antimicrobial effect, as the physical gel matrix can potentially limit its dispersion in the growth medium. Both concentrations were optimized based on preliminary screening to ensure reliable detection of antimicrobial activity. Streptomycin, a broad-spectrum aminoglycoside antibiotic, inhibits bacterial protein synthesis by binding to the 30S ribosomal subunit. Due to its efficacy against a wide range of bacterial species, including uncommon strains, it serves as an effective positive control in zone of inhibition assays (Table 2).

The minimum inhibitory concentration (MIC) of the metallogel Co-LS was determined against four bacterial strains. Distinct variations in antibacterial activity were observed among the tested strains. In the case of *B. subtilis*, strong zones of inhibition were observed starting at 80 µg/ml, with the zone diameter increasing progressively at higher concentrations. Complete inhibition of bacterial growth was achieved at 80 µg/ml and above, indicating that the MIC for *B. subtilis* is approximately 80 µg/ml. *S. aures* also showed marked susceptibility to the compound, with weak inhibition visible at 60 µg/ml and complete inhibition at 80 µg/ml, suggesting an MIC value of around 80 µg/ml.

By contrast, *E. coli* displayed moderate sensitivity. Inhibitory effect was noted only at 100 µg/ml, while lower concentrations (20–80 µg/ml) showed faint inhibition zones, indicating an MIC of approximately

View Article Online
DOI: 10.1039/D6MA00248J

100 µg/ml. *P. aeruginosa*, known for its intrinsic resistance to many antimicrobial agents, exhibited the least sensitivity toward the test compound. It produced a faint zone across the concentrations, whereas no clear inhibition was observed even at 100 µg/ml, suggesting partial resistance against Co-LS.

The control antibiotic, streptomycin, produced strong and well-defined zones of inhibition against all four bacterial species, validating the reliability of the assay and confirming the growth viability of the cultures.

Overall, the MIC values of the test compound were estimated to be 80 µg/ml for *B. subtilis*, 80 µg/ml for *S. aureus*, and 100 µg/ml for *E. coli*. These results suggest that the test compound possesses moderate to strong antibacterial potential, particularly against Gram-positive bacteria, and could serve as a promising candidate for further antimicrobial evaluation.

Table 2. Activity of positive control (antibiotic Streptomycin) against Bacterial strain(s).

Bacterial strain (s)	**Volume of antibiotic given as positive control (µL)**	**Concentration of antibiotic used as positive control (mg mL^{-1})**	**Zone of inhibition (mm in diameter)**
Escherichia coli	5	1	13±0.1
Bacillus subtilis	5	1	18.2±0.1
Pseudomonas aeruginosa	5	1	13±0.2
Staphylococcus aureus	5	1	19±0.15

Table 3. Activity of sample Co-LS against Bacterial strain(s).

Sl no.	Bacterial strain	Zone of inhibition (mm in diameter)					
		Positive control	**Concentration of Co-LS (mg ml^{-1})**				
			20mg/ml	**40mg/ml**	**60mg/ml**	**80mg/ml**	**100mg/ml**
1.	***Escherichia coli***	13±0.2	No zone	No zone	10 ±0.2	11±0.21	13±0.11

View Article Online
DOI: 10.1039/D6MA00248J

2.	***Bacillus subtilis***	18±0.22	No zone	No zone	No zone	10±0.22	13±0.15
3.	***Pseudomonas aeruginosa***	11±0.15	No zone	10±0.12	12±0.05	14±0.1	11±0.21
4.	***Staphylococcus aureus***	15±0.1	No zone	14±0.15	15±0.2	15±0.11	19±0.05

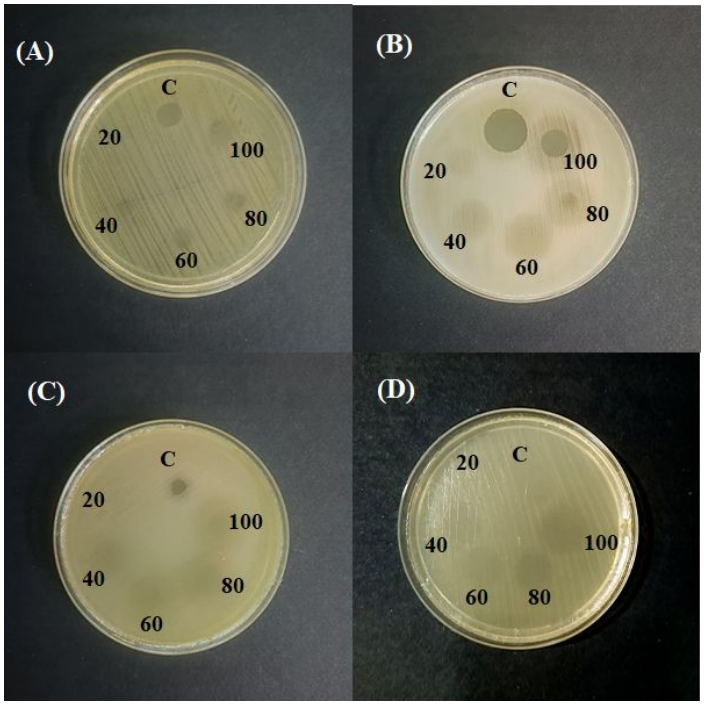

Fig. 11. Antimicrobial activity of Co-Ls across a series of concentrations against four bacterial strains: (A) *Escherichia coli,* (B) *Bacillus subtilis,* (C) *Pseudomonas aeruginosa,* and (D) *Staphylococcus aureus*. The different concentrations are 20 mg/ml, 40mg/ml, 60 mg/ml, 80mg/ml, 100 mg/ml.

.

4. Conclusions

In this work, we report the successful synthesis of a supramolecular Co(II)-metallohydrogel via a rapid, room-temperature mixing of cobalt nitrate hexahydrate and L-serine in an aqueous medium. FESEM revealed a well-defined, hierarchical flake-like network, while rheological measurements confirmed the gel's mechanical robustness. FT-IR spectroscopy identified key non-covalent interactions responsible for gel formation. The metallohydrogel exhibited semiconducting behaviour, as demonstrated by optical band-gap analysis and its performance in an ITO/Co-LS-PMMA/Al thin-film diode device, where it

View Article Online
DOI: 10.1039/D6MA00248J

showed distinct rectifying characteristics suited for optoelectronic applications. Notably, the gel also displayed potent antimicrobial activity, comparable to that of standard streptomycin, suggesting potential for pharmaceutical and biomedical use. This facile synthesis strategy offers a sustainable route for the development of multifunctional materials. Overall, the study presents a versatile platform for future advancements in healthcare, environmental technologies, and next-generation soft electronics through the rational design of supramolecular functional gels.

Conflicts of interest

The authors declare no competing financial interests.

Acknowledgements

S.S. is thankful to DST India, New Delhi for Inspire Fellowship (No. DST/inspire Fellowship/2022/IF220441). S.B. thankfully acknowledges DST Inspire Faculty Research Grant (Faculty Registration No.: IFA18-CH304; DST/INSPIRE/04/2018/000329).

Notes and references

1) D. Tripathy, A. S. Gadtya and S. Moharana, *Polym.-Plast. Technol. Mater.,* 2023, **62**, 306–326.
2) S. Datta and S. Bhattacharya, *Chem. Soc. Rev.,* 2015, **44**, 5596–5637.
3) A. Pape, M. Bastings, R. Kieltyka, H. Wyss, I. Voets, E. Meijer and P. Dankers, *Int. J. Mol. Sci.,* 2014, **15**, 1096–1111.
4) X. Ma and H. Tian, *Acc. Chem. Res.*, 2014, **47**, 1971–1981.
5) K. Karmakar, A. Dey, S. Dhibar, R. Sahu, S. Bhattacharjee, P. Karmakar, P. Chatterjee, A. Mondal and B. Saha, *RSC Adv.,* 2023, **13**, 2561–2569.
6) S. Ganta and D. K. Chand, *Dalton Trans.,* 2015, **44**, 15181–15188.
7) G. Yu, X. Yan, C. Han and F. Huang, *Chem. Soc. Rev.,* 2013, **42**, 6697.
8) S. Dhibar, S. K. Ojha, A. Mohan, S. P. C. Prabhakaran,S. Bhattacharjee, K. Karmakar, P. Karmakar, P. Predeep, A. K. Ojha and B. Saha, *New J. Chem.,* 2022, **46**, 17189–17200.
9) M. Shirakawa, N. Fujita and S. Shinkai, *J. Am. Chem. Soc.,* 2003, **125**, 9902–9903.
10) T.-A. Asoh and A. Kikuchi, *Chem. Commun.*, 2012, **48**, 10019.
11) X. Yang, H. Zhang, J. Zhao, Y. Liu, Z. Zhang, Y. Liu and Yan, *Chem. Eng. J., 2022*, **450**, 138135.
12) A. Rajak and A. Das, *ACS Polym. Au,* 2022, **2**, 223–231.
13) Y. Xu, Q. Wu, Y. Sun, H. Bai and G. Shi, *ACS Nano,* 2010, **4**,7358–7362.
14) S. Some, P. Das, S. Pal, S. Dhibar, D. Kumari, S. Bhattacharjee, S. J. Ray, T. O. Ajiboye, S. Dam, P. P. Ray and B. Saha, RSC Adv., 2025, 15, 18392–18402,
15) J. W. Steed, *Chem. Soc. Rev.,* 2010, **39**, 3686.
16) K. Hanabusa, K. Hiratsuka, M. Kimura and H. Shirai, *Chem. Mater.,* 1999, **11**, 649–655.
17) A. Prathap, K. M. Sureshan, *Langmuir,* 2019, **35**, 6005-6014.
18) A. Dawn and A. Ajayaghosh, *Chem. Soc. Rev.*, 2010, 39, 3687–3700.
19) H. Sigel and R. B. Martin, *Chem. Rev.*, 1982, **82**, 385–426..
20) S. Dhibar, A. Roy, P. Das, T. Sarkar, M. Goswami, S. Some, K Karmakar, P. Ruidas, S. Bhattacharjee, T. O. Ajiboye, A. S. Ray, K. Sarkar, S. J. Ray, B. Saha, *Mater. Adv.,* 2025, **6**, 1899-1913.

View Article Online
DOI: 10.1039/D6MA00248J

21) A. Roy, S. Dhibar, K. Karmakar, S. Bhattacharjee, B. Saha, S. J. Ray, *Scientific Reports,* 2024, **14**, 13109.

22) C. Wang, K. Xia, H. Zhang and X. Zhao, *Chem. Soc. Rev.*, 2017, **46**, 6764–6815.

23) K Karmakar, A. Roy, S. Dhibar; S. Majumder, S. Bhattacharjee, B. Mondal, S. M. Rahaman, R. Saha, S. J. Ray, B. Saha, *ACS Appl. Electron. Mater.,* 2023, **5**, 3340-3349.

24) M.-O. M. Piepenbrock, G. O. Lloyd, N. Clarke; J. W. Steed, *Chem Rev,* 2010, **110**, 1960-2004.

25) M. Suzuki and K. Hanabusa, *Chem. Soc. Rev.*, 2009, **38**, 967–975

26) S. Ganta, D. K. Chand, *Dalton Trans.,* 2015, **44**, 15181-15188.

27) C. Po, Z. Ke, A. Y. Tam, H. Chow, V. W. Yam. *Chem. Eur. J,* 2013, **19**, 15735-15744.

28) B. Jiang, L.-J. Chen, G.-Q. Yin, Y.-X. Wang, W. Zheng, L. Xu, H.-B. Yang, *Chem. Commun,* 2017, **53**, 172-175

29) S. Dhibar, A. Roy, P. Das, T. Sarkar, M. Goswami, S. Some, K. Karmakar, P. Ruidas, S. Bhattacharjee, T. O. Ajiboye, A. S. Ray, K. Sarkar, S. J. Ray and B. Saha, *Mater. Adv.*, 2025, **6**, 1899–1913.

30) S. Dhibar, A. Mohan, R. Laha, S. Some, P. Kaith, A. Trivedi, S. Bhattacharjee, L. N. Nthunya, T. O. Ajiboye, A. Bera, S. K. Panja, A. K. Das, S. Dam, P. Predeep and B. Saha, *RSC Adv.*, 2025, **15**, 33494–33505.

31) B. Pal, S. Dhibar, R. Mukherjee, S. Bhattacharjee, P. P. Ray, B. Saha, *Mater. Adv.,* 2023, **4**, 3628-3635.

32) S. Datta and P. Dastidar, Chem. Soc. Rev., 2022, 51, 5580–5631.

33) S. Dhibar, A. Mohan, S. Babu, S. Bhattacharjee, S. Some, S. J. Ray, S. Roy, T. O. Ajiboye, P. Predeep and B. Saha, *Discov. Mol.*, 2025, **2**, 13,

34) W.-L. Guan, K. M. Adam, M. Qiu; Y.-M. Zhang, H. Yao, T.-B. Wei, Q. Lin, *Supramol Chem,* 2020, **32**, 578-596.

35) E. M. M. Ibrahim, L. H. Abdel-Rahman, A. M. Abu-Dief, A. Elshafaie, S. K. Hamdan, A. M. Ahmed, *Mater Res Bull,* 2018, **107**, 492-497.

36) E. M. M. Ahmed, L. H. Abdel-Rahman, A. M. Abu-Dief, A. Elshafaie, S. K. Hamdan, A. M. Ahmed, *Phys. Scr.,* 2018*, 93* 055801

37) S. Khodami, K. Kaniewska, J. Romanski, M. Karbarz, Z. Stojek, *ACS Omega,* 2025, **10**, 12062-12075.

38) H. Sigel and R. B. Martin, *Chem. Rev.*, 1982, *82*, 385–426.

39) H. Sigel (ed.), *Metal Ions in Biological Systems*, Vol. 2, Marcel Dekker, New York, 1973.

40) T. Shao, N. Falcone and H.-B. Kraatz, *ACS Omega*, 2020, 5, 1312–1317.

41) S. K. Cheung, N. W. Cheung, *Appl. Phys. Lett.,* 1986*,* **49**, 85-87.

42) P. N. Murgatroyd, *J. Phys. D. Appl. Phys.,* 1970, **3**, 151-156.

43) D. Joung, A. Chunder, L. Zhai, S. I. Khondaker, *Appl. Phys. Lett.,* 2010, **97**, 093105

44) S. Dhibar, S. Some, S. Pal, R. Laha, P. Kaith, A. Trivedi, S. Bhattacharjee, L. N. Nthunya, T. O. Ajiboye, S. K. Panja, A. K. Das, A. Bera, S. Dam and B. Saha, *RSC Adv.*, 2025, **15**, 27544–27550

45) H. Sirringhaus, *Adv. Mater.*, 2014, 26, 1319–1335.

46)) V. Podzorov, *Nat. Mater.*, 2013, 12, 443–444

View Article Online
DOI: 10.1039/D6MA00248J

Data Availability Statement

The authors declare that the data supporting the findings of this study are available within the paper and its Electronic Supplementary Information files. Should any raw data files be needed in another format they are available from the corresponding author upon reasonable request.